Published November 11, 2013

Peregrination of the selectivity filter delineates the pore of the human voltage-gated proton channel hH_V1

Deri Morgan,[1] Boris Musset,[1] Kethika Kulleperuma,[2,3] Susan M.E. Smith,[4] Sindhu Rajan,[5] Vladimir V. Cherny,[1] Régis Pomès,[2,3] and Thomas E. DeCoursey[1]

[1]Department of Molecular Biophysics and Physiology, Rush University, Chicago, IL 60612
[2]Molecular Structure and Function, Hospital for Sick Children, Toronto, Ontario M5G 1X8, Canada
[3]Department of Biochemistry, University of Toronto, Toronto, Ontario M5S 1A1, Canada
[4]Department of Biology and Physics, Kennesaw State University, Kennesaw, GA 30144
[5]Department of Medicine, University of Chicago, Chicago, IL 60637

Extraordinary selectivity is crucial to all proton-conducting molecules, including the human voltage-gated proton channel (hH_V1), because the proton concentration is $>10^6$ times lower than that of other cations. Here we use "selectivity filter scanning" to elucidate the molecular requirements for proton-specific conduction in hH_V1. Asp^{112}, in the middle of the S1 transmembrane helix, is an essential part of the selectivity filter in wild-type (WT) channels. After neutralizing Asp^{112} by mutating it to Ala (D112A), we introduced Asp at each position along S1 from 108 to 118, searching for "second site suppressor" activity. Surprisingly, most mutants lacked even the anion conduction exhibited by D112A. Proton-specific conduction was restored only with Asp or Glu at position 116. The D112V/V116D channel strikingly resembled WT in selectivity, kinetics, and ΔpH-dependent gating. The S4 segment of this mutant has similar accessibility to WT in open channels, because R211H/D112V/V116D was inhibited by internally applied Zn^{2+}. Asp at position 109 allowed anion permeation in combination with D112A but did not rescue function in the nonconducting D112V mutant, indicating that selectivity is established externally to the constriction at F150. The three positions that permitted conduction all line the pore in our homology model, clearly delineating the conduction pathway. Evidently, a carboxyl group must face the pore directly to enable conduction. Molecular dynamics simulations indicate reorganization of hydrogen bond networks in the external vestibule in D112V/V116D. At both positions where it produces proton selectivity, Asp frequently engages in salt linkage with one or more Arg residues from S4. Surprisingly, mean hydration profiles were similar in proton-selective, anion-permeable, and nonconducting constructs. That the selectivity filter functions in a new location helps to define local environmental features required to produce proton-selective conduction.

INTRODUCTION

Voltage-gated proton channels (H_V1s) enable phagocytes to kill pathogens (Henderson et al., 1988; DeCoursey et al., 2003; Morgan et al., 2009; DeCoursey, 2010; Demaurex, 2012), basophils to secrete histamine (Musset et al., 2008b), and airway epithelia to control surface pH (Fischer, 2012), as well as enable sperm motility (Musset et al., 2012) and capacitation (Lishko et al., 2010), and B lymphocyte signaling (Capasso et al., 2010), and may exacerbate breast cancer metastasis (Wang et al., 2012) and ischemic brain damage (Wu et al., 2012). All of these functions are predicated on the proton specificity of H_V1. The low concentration of H^+ in biological fluids means that extraordinary selectivity is necessary even to ensure that H^+ is the main conducted species. In fact, proton selectivity in H_V1 appears to be perfect (Musset et al., 2011; DeCoursey, 2013).

An acidic group in the middle of the S1 transmembrane segment is critical to the proton specificity of H_V1 and is provided by Asp^{112} in human H_V1 (hH_V1; Musset et al., 2011) and Asp^{51} in H_V1 from a dinoflagellate, *Karlodinium veneficum* (Smith et al., 2011). Despite only 15% amino acid identity of the proteins, the conservative Asp→Glu mutation preserved proton specificity, whereas Ser, Ala, or His substitution for Asp at this position resulted in anion permeability in both species, strongly suggesting that the selectivity mechanism is widely conserved evolutionarily. The presence of an Asp facing the pore is not sufficient, however, because Asp^{185} can be neutralized without compromising proton selectivity, and does not preserve selectivity when Asp^{112} is neutralized (Musset et al., 2011). Other molecular elements that may be required are not known. Our homology model indicates that the second of three Arg residues in

D. Morgan and B. Musset contributed equally to this paper.
Correspondence to Thomas E. DeCoursey: tdecours@rush.edu

Abbreviations used in this paper: EC, extracellular; hH_V1, human voltage-gated proton channel; H_V1, voltage-gated proton channel; IC, intracellular; MD, molecular dynamics.

The Rockefeller University Press $30.00
J. Gen. Physiol. Vol. 142 No. 6 625–640
www.jgp.org/cgi/doi/10.1085/jgp.201311045

Supplemental Material can be found at:
http://jgp.rupress.org/content/suppl/2013/11/05/jgp.201311045.DC1.html
http://jgp.rupress.org/content/suppl/2014/01/24/jgp.201311045.DC2.html

Published November 11, 2013

the S4 segment, Arg^{208}, forms a salt bridge with Asp^{112}, and that the resulting charge compensation is important for proton selectivity (Kulleperuma et al., 2013). To refine further the molecular requirements of the selectivity filter, we explore here the extent to which the critical Asp can be moved along the S1 segment. We find that an excellent proton channel is produced when Asp is shifted from position 112 to position 116. The mutant channel is proton specific, exhibits ΔpH-dependent gating characteristic of all H_V1s, and surprisingly, neutral amino acid substituents at this location produce anion permeability. Molecular dynamics (MD) simulations indicate that Asp^{116} forms a salt bridge with Arg^{205} and/or Arg^{208}, but the latter also pairs with Asp^{185}, reflecting reorganization of charge clusters in the mutant compared with WT channels. The results underline the importance of intramolecular charge compensation for proton selectivity.

MATERIALS AND METHODS

Gene expression

Site-directed mutants were created using the Stratagene QuikChange (Agilent Technologies) procedure according to the manufacturer's instructions. Transfection was done as described previously (Kulleperuma et al., 2013). Both HEK-293 cells and COS-7 cells were used as expression systems, the latter more frequently. In a previous study, we systematically compared the properties of hH_V1 when expressed in these two cell lines and found no difference (Musset et al., 2008a). Although currents that decayed at large positive voltages (presumed to be volume-regulated anion currents) were sometimes seen at the start of experiments, these disappeared over time. Occasional cells displayed a few unidentified single-channel currents superimposed on the macroscopic currents. The unitary conductance of hH_V1 is just 140 fS at pH_i 5.5 (Cherny et al., 2003); thus, visible unitary currents were considered extraneous and were ignored. No other voltage- or time-dependent conductances were observed under the conditions of this study. Thus, depolarization-activated time-dependent currents, which in many cells were orders of magnitude larger than any background currents, were assumed to reflect the transfected construct. Both cell lines sometimes exhibit small native H_V1 currents, which could be distinguished from transfected mutant channels by their high Zn^{2+} sensitivity (see Results).

Electrophysiology

GFP-tagged proton channels were identified using inverted microscopes (Nikon) with fluorescence capability. Conventional patch-clamp techniques were used at 21°C or at room temperature (20–25°C) (Kulleperuma et al., 2013). Bath and pipette solutions contained 60–100 mM of buffer, 1–2 mM $CaCl_2$ or $MgCl_2$ (intracellular [IC] solutions were Ca^{2+} free), 1–2 mM EGTA, and $TMAMeSO_3$ to adjust the osmolality to ∼300 mOsm, titrated with TMAOH. Buffers used were Mes at pH 5.5–6.0, HomoPIPES at pH 4.5, and PIPES at pH 7.0. For Zn^{2+} measurements, EGTA was omitted. Currents are shown without leak correction. Reversal potentials were corrected for measured liquid junction potentials. Unless stated otherwise, cells were held at a holding potential, V_{hold}, before pulses and returned to V_{hold} after families of pulses.

Reversal potentials were determined by two methods, depending on the relative positions of $V_{threshold}$ and V_{rev}. For most constructs, $V_{threshold}$ was positive to V_{rev}, and the latter was determined by examining tail currents (e.g., Fig. 2 B). Because hH_V1 currents were the only time-dependent conductance present, estimates of the amplitude and direction of current decay during deactivation were used to establish V_{rev} (Morgan and DeCoursey, 2007). By this procedure, time-independent leak or other extraneous conductances do not affect V_{rev}. For mutants in which $V_{threshold}$ was negative to V_{rev} (for example, D112A/V116D in Fig. 2 C), it was possible to observe the reversal of the direction of currents activated during pulse families. Tail currents were not observed in nontransfected cells; for example, Fig. 1 B illustrates the absence of tail currents in a cell with the nonconducting D112V mutant.

MD simulations

MD simulations of the WT protein, single-point mutants D112V and D112S, and double-point mutants D112V/V116D ("VD") and D112V/V112S ("VS") were performed in a hydrated lipid bilayer based on the homology model constructed and validated in a recent study (Kulleperuma et al., 2013).

12 conformations of the WT protein with pore-associated water were used as initial structures. These snapshots correspond to the endpoint of 12 different 200-ns-long unrestrained simulations in a membrane-mimetic octane slab (Kulleperuma et al., 2013). Each conformation represents one of the three configurations of the D112-R208 salt bridge: bidentate and monodentate conformations (involving two or one hydrogen bond, respectively), and open, in order of increasing separation. A preequilibrated configuration of a 1-palmitoyl-2-oleoylphosphatidylcholine (POPC) bilayer was obtained from a previous study (Kulleperuma et al., 2013). The OPLS-AA protein force field (Jorgensen et al., 1996) was mixed with the Berger lipid parameters (Berger et al., 1997) by applying the half-ε double-pairlist method (Chakrabarti et al., 2010). The TIP3P water model was used (Jorgensen et al., 1983). InflateGRO (Kandt et al., 2007) was used to embed the protein in the bilayer. The system was then hydrated, and 54 Na^+ and 56 Cl^- ions were added to neutralize the charge of the system and yield an approximate ionic concentration of 500 mM. The resulting simulator cell consisted of 126 POPC and ∼5,900 water molecules in a box of $\sim 6.5 \times 6.5 \times 8\ nm^3$. The MD parameters used for this study are described elsewhere (Kulleperuma et al., 2013).

Each of the 12 WT systems was first energy-minimized using 50,000 steps of steepest descent, followed by an equilibration phase of 50 ns with position restraints on protein backbone and pore-associated water oxygen atoms. The production run consisted of 200-ns-long unrestrained simulations for each system. Snapshots of protein and pore-associated water molecules were selected from each of the 12 equilibrated WT protein systems at $t = 100$ ns to produce single- and double-point mutants. Mutations were introduced using an in-house script, followed by 1,000 steps of energy minimization. Asp^{112} and Val^{116} side chains were modified to Val, Ser, or Glu by either overwriting the WT heavy atoms or deleting some or both. Side-chain and backbone dihedral angles were checked after energy minimization. Extra ions were added to the solution as required to neutralize the system after mutations were introduced. Another 50,000 steps of energy minimization were performed before an equilibration phase consisting of an additional 25 ns with position restraints, as described above. 12 time trajectories of 200 ns differing in the initial conformation of the protein were generated for each mutant. The total production time was 12 μs. For the final analysis, eight replicas of WT and VD and seven replicas of VS, D112V, and D112S were selected after discarding replicas that displayed significant changes in secondary structure.

Snapshots saved every 20 ps during the last 100 ns of each selected production run were analyzed for each system. Molecular graphics were generated by VMD 1.8.7 (Humphrey et al., 1996), and all trajectories were analyzed using Gromacs tools and in-house codes.

Published November 11, 2013

Online supplemental material

Figs. S1 and S2 illustrate the structural plasticity of the channel with respect to translation of the four transmembrane helices during extended MD simulations. Table S1 provides V_{rev} data for D112V/V116D and D112V/V116D/R211H mutants in the presence of several cations or Cl^- that show both constructs to be proton selective. The online supplemental material is available at http://www.jgp.org/cgi/content/full/jgp.201311045/DC1.

RESULTS

We generated a series of mutants in which the Asp residue critical to proton specificity was effectively shifted up and down the S1 helix to each position from 108 to 118. In the initial series of experiments, we replaced Asp^{112} with Ala (D112A) to produce an anion-permeable channel (Musset et al., 2011), and then introduced a second mutation with the goal of restoring proton selectivity ("second site suppression"). Additional studies were done in the D112V background, which in a sense is more rigorous, because this single mutant does not conduct at all (Musset et al., 2011). All mutations were introduced into a Zn^{2+}-resistant background (H140A/H193A), so that spurious small native H_V1 currents often present in COS-7 or HEK-293 cells (Musset et al., 2011) could be identified by their sensitivity to 10 µM Zn^{2+}. Distinct Zn^{2+}-insensitive currents were observed only in mutants with Asp at positions 116 or 109 (D112A/V116D, D112A/V109D).

The second site mutation V116D restores proton selectivity to nonconducting or anion-permeable mutants

Fig. 1 shows that although the single-point mutation D112V eliminates current altogether (Musset et al., 2011), introducing Asp at position 116 restores robust proton current to the double mutant, D112V/V116D. Similarly, the D112A single mutant is anion permeable (Musset et al., 2011), but introducing Asp at position 116 restored proton-specific current to the double mutant, D112A/V116D. The proton selectivity of both double mutants, D112A/V116D and D112V/V116D, was confirmed by the proximity of their reversal potentials, V_{rev}, to the Nernst potential for H^+, E_H (Fig. 2 A), over a wide pH range (pH_o 4.5–7.5 and pH_i 5.5–7.0). Fig. 2 B illustrates determination of V_{rev} from tail currents in a cell with D112V/V116D channels at pH_o 5.5 and 7.0, with pH_i 5.5. As indicated by the arrows, V_{rev} shifted from 0 to −77 mV, near E_H of −87 mV. The D112A/V116D mutant activated in a more negative voltage range so that inward currents were observed negative to E_H in families of currents. Fig. 2 C illustrates currents from pulses bracketing V_{rev} that reveal an ∼60-mV shift between pH_o 5.0 and 6.0. In addition, substituting Na^+, Li^+, or K^+ for TMA^+, or Cl^- for $CH_3SO_3^-$ had no effect on V_{rev} (Table S1). In summary, shifting Asp from position 112 to 116 moves the proton selectivity filter outward by one turn of the helix.

Asp supports current only when facing the pore

Surprisingly, moving Asp to positions other than 109 or 116 eliminated voltage-gated current altogether. All mutants were tagged with GFP, and transfected cells with green "halos" indicating membrane expression were selected under fluorescence for recording. Nonconducting Asp mutants included (mutation, number of cells): positions 108 (D112A/L108D, 10), 110 (D112A/V110D, 4), 111 (D112A/L111D, 4), 113 (D112A/A113D, 5), 114 (D112A/L114D, 4), 115 (D112A/L115D, 4), 117 (D112A/L117D, 7), and 118 (D112A/A118D, 4). Positions 116, 112, and 109 (Fig. 1, cartoon) all face the "pore" in the predicted open-state structure of hH_V1 (Kulleperuma et al., 2013). Evidently, Asp at a nonpore-facing location fails to support conductance, confirming that positions 109, 112, and 116 line the pore of hH_V1.

As a control for the possibility that nonconducting mutants did not fold properly, we created a single mutant, A113D, in which the native Asp^{112} was preserved. If Asp at a nonpore-facing location caused the protein to misfold, A113D should not conduct. Instead, A113D displayed small voltage-gated currents that were kinetically different from WT currents but were unequivocally

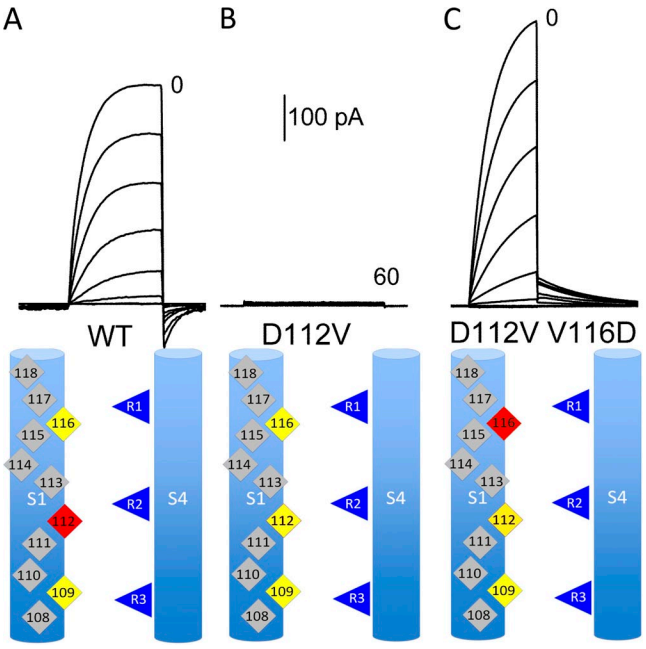

Figure 1. The D112V mutation abolishes current, but V116D restores proton-specific current, an example of second-site suppression. Whole-cell currents at pH_o 7.0 and pH_i 5.5 during pulses in 10-mV increments up to the indicated voltages for WT (A), D112V (B), or D112V/V116D (C), all expressed in COS-7 cells. Holding potential (V_{hold}) and pulse durations were −90 mV, 1 s (A), −40 mV, 3 s (B), and −60 mV, 2 s (C). In all cases, the voltage was returned to V_{hold} after the pulse, which is why the tail currents are inward for A and outward for C. Cartoons in all figures indicate S1 and S4 helices, with color coding as follows: red, Asp or Glu; yellow, Val; blue, Arg; gray, other amino acids or nonpore-facing residues.

Published November 11, 2013

proton selective (Fig. 3). Thus, nonconducting mutants, including D112A/A113D, most likely were expressed but nonfunctional. If, despite the appearance of green protein in the membrane, some mutants misfolded, the fact remains that these proteins do not function as channels.

At position 109, Asp plays a permissive role

Introducing Asp at position 109 into the nonconducting D112V background (Musset et al., 2011) did not overcome the lack of conductance produced by the D112V single mutation ($n = 8$ cells). However, the D112A/V109D mutant exhibited distinct currents at pH_o 5.5 and pH_i 5.5 (Fig. 4 A), in contrast to the majority of mutants that did not conduct (D112A/L108D, D112A/V110D, D112A/L111D, D112A/A113D, D112A/L114D, D112A/L115D, D112A/L117D, and D112A/A118D). Replacing $CH_3SO_3^-$ with Cl^- increased the outward current (Fig. 4 C), reflecting Cl^- influx, and produced a large negative shift of V_{rev} (Fig. 4, B vs. D), confirming Cl^- permeability. The shift of V_{rev} when Cl^- replaced $CH_3SO_3^-$ was -35.9 ± 4.2 mV (SEM; $n = 5$), in the range reported for the D112A single mutant, -29 mV (Musset et al., 2011). Evidently, introducing Asp at position 109 did not interfere with anion conduction seen in the D112A single mutant (Musset et al., 2011). Both the anion selectivity of D112A/V109D and the lack of conductance in D112V/V109D suggest that at position 109, Asp cannot mediate proton selectivity and has no discernible effect on the selectivity that is established elsewhere. The two positions where Asp produced proton selectivity are in the external vestibule in our model, outside the highly conserved charge transfer center delimiter Phe^{150} (Tao et al., 2010).

The engineered Asp^{116} proton channel functionally resembles WT

To what extent does moving the selectivity filter outward by one turn of the helix reinstate native hH_V1 properties? The gating and pH dependence of the D112A/V116D and D112V/V116D mutants are illustrated in Fig. 5. The general appearance of the proton currents is unremarkable; the voltage dependence and gating kinetics are roughly similar to WT. In D112V/V116D, the time constant of tail current decay, τ_{tail}, was 1.1 ± 0.02 s (mean ± SEM; $n = 3$) at -40 mV and pH

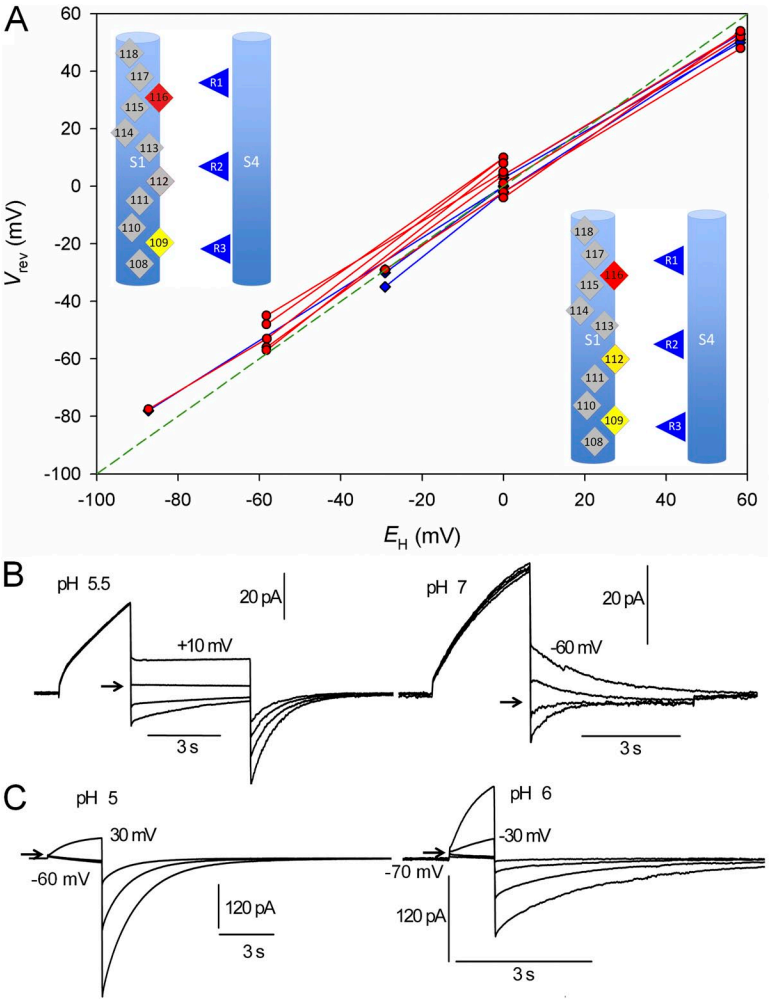

Figure 2. Second site suppression in double mutants. (A) Shifting the crucial aspartate from position 112 to 116 (V116D) restores proton selectivity to both the nonconducting D112V (red symbols) and the anion-permeable D112A (blue symbols) single mutants. Measurements in the same cell are connected by lines. For both, V_{rev} measured over a wide range (for D112V/V116D pH_o was 5.5, 6.0, 6.5, 7.0, 7.5, or 8.0, and pH_i was 5.5, 6.0, 6.5, or 7.0; for D112A/V116D pH_o was 4.5, 5.5, 6.0, 6.5, or 7.0, and pH_i was 5.5, 6.0, or 6.5) falls close to the Nernst potential for H^+, E_H (dashed green line). (B) Determination of V_{rev} from tail currents for D112V/V116D in a COS-7 cell with pH_i 5.5. Prepulses to +30 mV, pH_o 5.5, or to -40 mV, pH_o 7.0, activated the conductance, followed by repolarization to the indicated voltages in 10-mV increments, with the most positive labeled. (C) Determination of V_{rev} from current families for D112A/V116D in a COS-7 cell with pH_i 5.5. As indicated, V_{hold} was -60 mV (left) or -70 mV (right); the voltage was returned to V_{hold} after the pulses. Currents are shown during selected pulses that bracket V_{rev} in 10-mV increments. Inward current was activated negative to V_{rev}, and the first outward current is labeled.

Published November 11, 2013

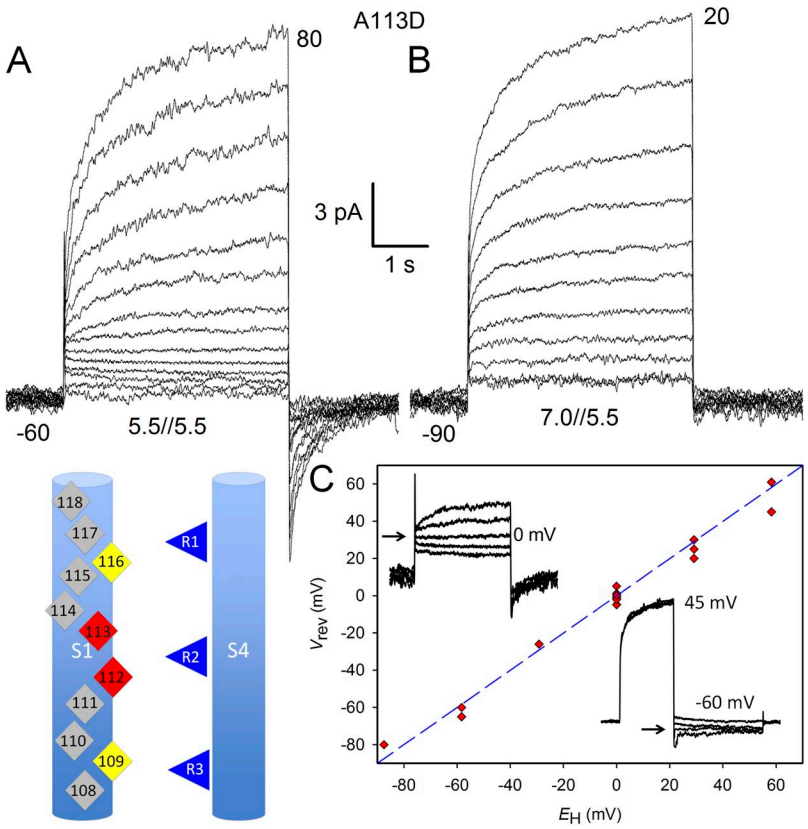

Figure 3. Introducing Asp at position 113, predicted by our model to be in a nonpore-facing location, results in membrane expression of a functioning proton-selective channel. The cartoon emphasizes that Asp^{112} is still present. Families of currents are shown in a COS-7 cell in whole-cell configuration at pH_o 5.5 (A) or 7.0 (B), with pH_i 5.5, with pulses applied from V_{hold} as labeled to the indicated voltages in 10-mV increments. Cells were returned to V_{hold} after pulses. (C) Proton selectivity is shown by the proximity of V_{rev} to E_H (dashed line). Insets show V_{rev} determination (left) at pH_o 5.5 and pH_i 5.5 by reversal of current during a family of pulses in 10-mV increments (V_{hold} = −60 mV) and at pH_o 7.0 and pH_i 5.5 (right) by tail currents. V_{rev} was measured at pH_o 4.5, 5.0, 5.5, 6.5, 7.0, and 7.5, and at pH_i 5.5 or 6.5.

5.5//5.5, which is close to the WT value of 0.81 s measured under the same conditions (Musset et al., 2011). The activation time constant, τ_{act}, was 2.3 ± 0.3 s (n = 3) at +40 mV in D112V/V116D, compared with the WT value of 1.1 s (Musset et al., 2011). Thus, marked changes in the gating of the mutant channels were not observed.

A characteristic property shared by all known H_V1 is tight regulation of the position of the g_H–V relationship by the pH gradient, ΔpH (Cherny et al., 1995;

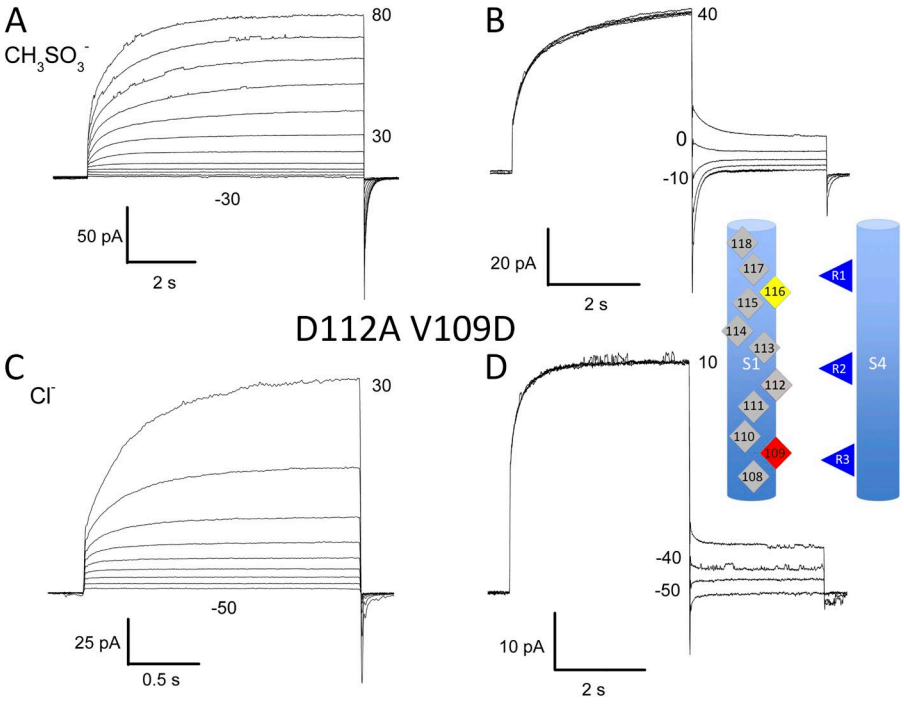

Figure 4. Moving aspartate from position 112 to 109 results in anion currents. Whole-cell currents in a COS-7 cell expressing D112A/V109D channels, all at pH_o 5.5 and pH_i 5.5, in symmetrical TMA^+ $CH_3SO_3^-$ (A and B) or with Cl^- in the bath (C and D). Pulses applied in 10-mV increments. V_{hold} was −40 mV (A and B) or −60 mV (C and D). Cells were returned to V_{hold} after pulses. V_{rev} determination from tail currents (B and D), with pulses in 10-mV increments.

Published November 11, 2013

DeCoursey, 2013). Because the mechanism remains mysterious, we examined this property. As evident in Fig. 5 (D and E), changes in pH_o produced shifts in both I_H–V and g_H–V curves of roughly 40 mV/U, similar to the shifts observed in native and WT hH_V1s (Ramsey et al., 2006; Musset et al., 2008a). Plots of $V_{threshold}$ versus V_{rev} for D112V/V116D (Fig. 5, D and E, red) and D112A/V116D (blue) had slopes (0.64 and 0.63, respectively) similar to those observed previously for WT hH_V1s (Musset et al., 2008a). The D112A/V116D mutant activated at voltages 26 mV more negative than D112V/V116D, suggesting relative stabilization of the open state by Ala versus Val at position 112. As a consequence of this shift, $V_{threshold}$ in D112A/V116D was often negative to E_H so that inward currents were observed. Nevertheless, ΔpH-dependent gating was preserved in both double mutants.

Mutations at position 116 (in D112V channels) mimic mutations at 112

That proton selectivity was restored to D112V and D112A mutants by introducing Asp at position 116 suggests that the intramolecular interactions at both positions that contribute to proton selectivity are similar. To explore the extent of equivalence of these positions, we compared effects of several other mutations at 116 with those at 112. Fig. 6 shows that robust proton-selective currents were observed when Glu replaced Asp at position 116 (in the D112V background), just as with replacement of Asp by Glu at position 112 (Musset et al., 2011). We found previously that neutral mutants of Asp^{112} were anion selective (Musset et al., 2011). Astoundingly, both Asn and Ser at position 116 produced anion-permeable channels in the D112V background, which itself does not conduct. Fig. 7 illustrates a current family

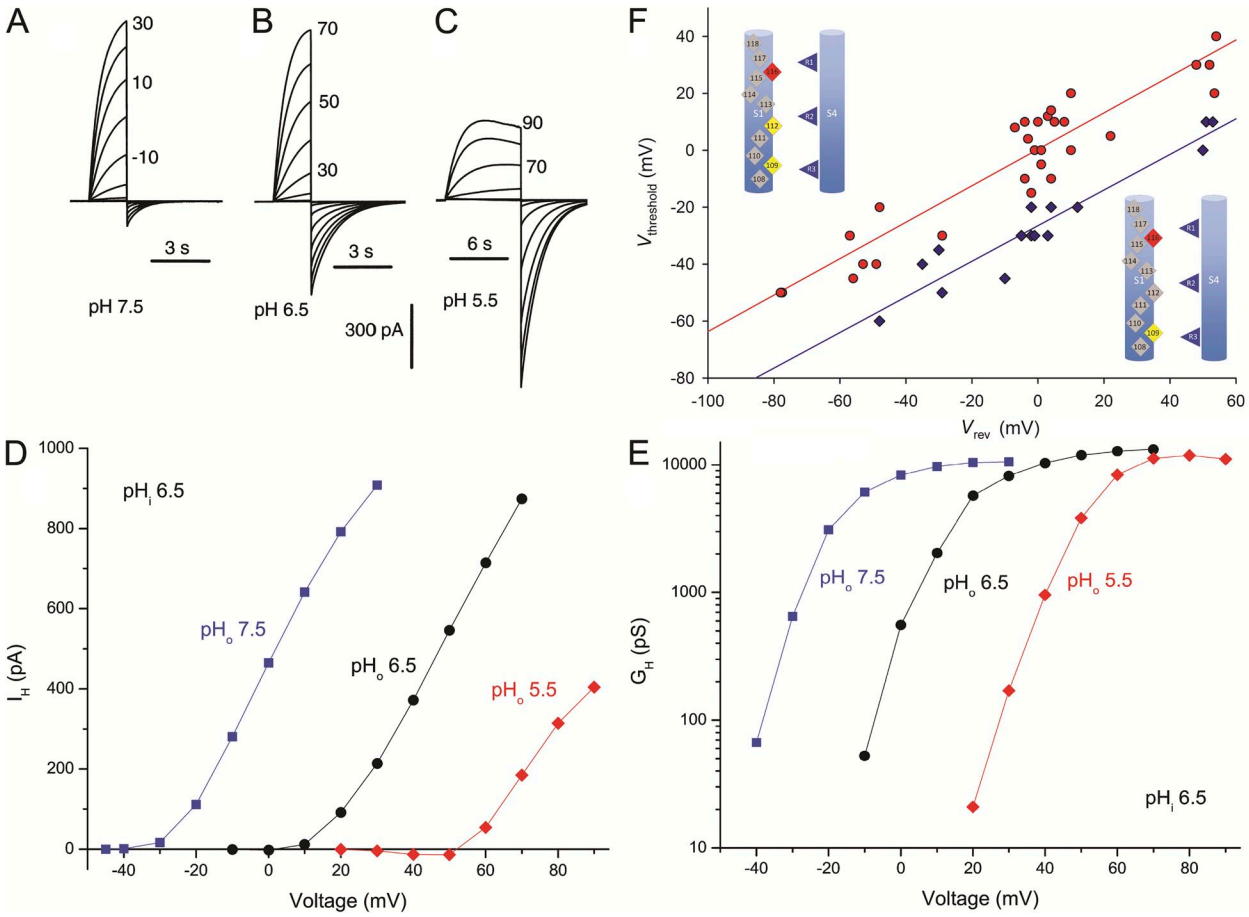

Figure 5. Voltage and pH dependence of gating of hH_V1 mutants with the selectivity filter shifter from 112 to 116. Families of currents in a COS-7 cell expressing D112A/V116D channels at pH_i 6.5 and pH_o 7.5 (A), 6.5 (B), or 5.5 (C) are shown in 10-mV increments as labeled, from V_{hold} −60 mV (A) or −30 mV (B and C). Cells were returned to V_{hold} after pulses. (D) Current–voltage relationships in this cell. Currents were fitted to a rising exponential function and extrapolated to infinite time. Note inward currents at pH_o 5.5. (E) Conductance–voltage relationships for the same currents. Limiting slope conductance for the most negative voltages provides a gating charge estimate of 5.3–6.0 e_0. (F) Regulation of voltage gating by ΔpH. $V_{threshold}$ is plotted against V_{rev} measured in the same cell and solution. Lines show linear regression fits defined by $V_{threshold} = 0.64\ V_{rev} + 0$ mV (D112V/V116D; red circles) or $V_{threshold} = 0.63\ V_{rev} - 26$ mV (D112A/V116D; blue diamonds).

Published November 11, 2013

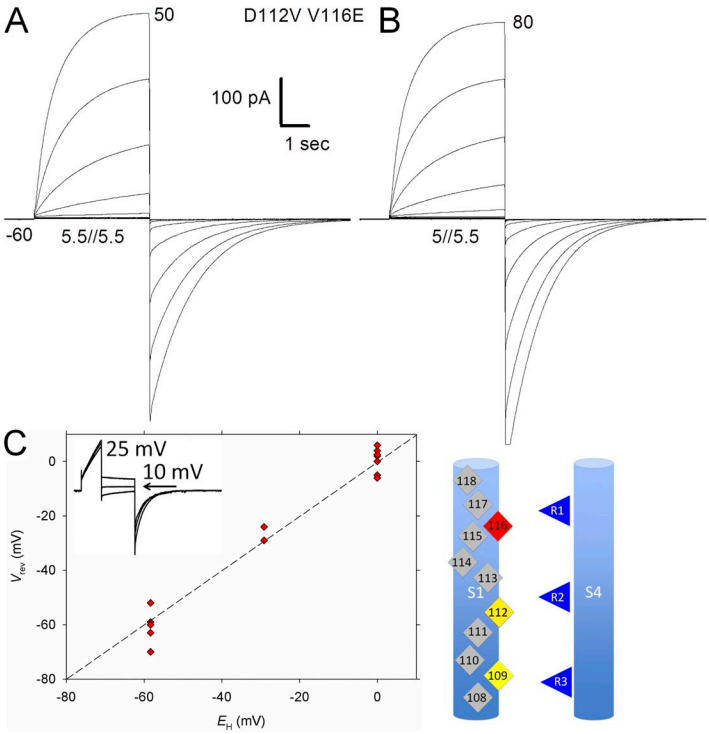

Figure 6. The D112V/V116E mutant is a functional proton-selective channel. (A) Families of currents generated by D112V/V116E in a HEK-293 cell in 10-mV increments at pH_o 5.5 and pH_i 5.5 (A), and pH_o 5.0 and pH_i 5.5 (B). As indicated, V_{hold} was −60 mV, and the membrane was returned to V_{hold} after pulses. (C) V_{rev} measured at pH_o 5.0, 5.5, 6.5, 7.0, and 7.5, and at pH_i 5.5 or 6.5, indicates that D112V/V116E is proton selective. Inset shows tail currents at 10 (uppermost), 5, and 0 mV at pH_o 5.5 and pH_i 5.5. Proton selectivity is imparted by either Asp or Glu at positions 112 or 116, indicating that side-chain length is not critical for this function.

in a cell with D112V/V116S in symmetrical pH 5.5 $TMACH_3SO_3$ solutions (Fig. 7 A), with V_{rev} near 0 mV (Fig. 7 B). Replacing bath $CH_3SO_3^-$ with Cl^- increased the outward current (Fig. 7 C) and shifted V_{rev} strongly negatively (Fig. 7 D): on average, by −37.0 ± 2.4 mV (mean ± SEM; $n = 7$) for Asn and −35.8 ± 1.8 mV ($n = 4$) for Ser. These values are similar to those obtained previously for single mutants D112N and D112S upon Cl^- addition: −33.1 and −40.8 mV, respectively (Musset et al., 2011). Thus, the introduction of Glu, Ser, or Asn at position 116 conferred permeability onto the nonconducting D112V mutant, in each case recapitulating the selectivity of the corresponding single mutations at position 112. Viewed in terms of the ability of a single–amino acid substituent to produce anion or proton selectivity, positions 112 and 116 were identical.

Zn^{2+} sensitivity of Arg→His mutants shows S4 position in open channels

It seemed possible that shifting the selectivity filter outward might alter the position of S4 in open channels. As a frame of reference, R211H currents were found previously to be sensitive to internal but not external Zn^{2+} during depolarizing pulses, suggesting that Arg^{211} remains

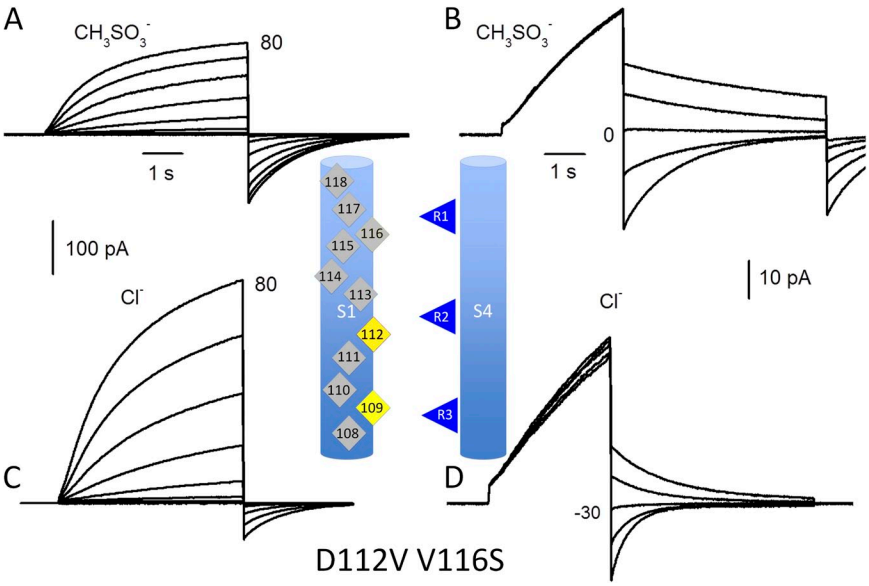

Figure 7. The D112V/V116S mutant is permeable to Cl^-. Replacing $CH_3SO_3^-$ with Cl^- increased outward current in families (A and C) and shifted the tail current reversal potential negatively (B and D). All measurements were in a COS-7 cell at symmetrical pH 5.5 with TMA^+ $CH_3SO_3^-$ solutions or external TMA^+ Cl^- solutions, as indicated. Pulses were applied in 10-mV increments from −40 to 80 mV for families and in 10-mV increments for tail currents as indicated. The cell was held at −30 mV and returned to V_{hold} after pulses. The same calibration bars apply to families (A and C) and tail currents (B and D).

Published November 11, 2013

internally accessible in the open state (Kulleperuma et al., 2013). The third Arg in S4 of the *Ciona* H_V1 was reported to be internally accessible in closed but not open channels (Gonzalez et al., 2010), perhaps reflecting the large size of the MTSET probe. Internal accessibility of position 211 in the filter-shifted R211H/D112V/V116D mutant was evaluated by testing the Zn^{2+} sensitivity of inside-out patches. This construct was proton selective (Table S1). In nine patches with R211H/D112V/V116D, 10 µM Zn^{2+} was introduced into the bath at pH_i 7.0, and test pulses were applied. The H^+ current was inhibited by 90.0 ± 3.6% (mean ± SEM), significantly ($P < 0.0001$ by unpaired *t* test) more than 29.7 ± 6.8% in six control patches (D112V/V116D). These results show that the 211 position is accessible to internally applied Zn^{2+}, but they do not distinguish whether the site is accessible in closed or open channels.

Accessibility of His^{211} in R211H/D112V/V116D channels in the open state was evaluated by adding Zn^{2+} or EGTA during pulses. In Fig. 8 A, shortly after the start of a pulse, 10 µM Zn^{2+} was introduced (red record), producing slowly progressing block. The subsequent pulse (Fig. 8 A, blue) illustrates the full extent of inhibition. Given that the probability of being open is high during large pulses—95% at pH_i 5.5 and 75% at pH_i 6.5 (Cherny et al., 2003)—and that gating is slow, cycling of channels through closed states during the pulse seems unlikely. Because Zn^{2+} must diffuse through the unstirred volume at the tip of the pipette to reach the membrane, onset of block was slow and likely dependent on pipette and patch geometry, but was observed unequivocally in four patches during long pulses. The addition of EGTA during a pulse to remove Zn^{2+} resulted in rapid reversal of block (Fig. 8 B) in six patches. The application of 10 µM Zn^{2+} to inside-out patches from cells expressing the control construct D112V/V116D produced comparatively minor effects on the current (Fig. 8 C), reminiscent of its effects on native H_V1 (Cherny and DeCoursey, 1999). Thus, His at position 211 in R211H/D112V/V116D was accessible to the internal solution even in the open state, indicating similar accessibility of the S4 Arg residues in open channels with the selectivity filter at either position 112 or 116.

Introducing Asp into S2 or S3 did not support proton conduction

Given that Asp can produce proton selectivity at two locations on S1, we moved Asp to several positions in the S2 or S3 transmembrane segments, always in the nonconducting D112V background. We chose five locations in the outer vestibule (S143D, I146D, L147D, V178D, and S181D) that face the pore in our model and are located roughly between the levels of positions 112–116. Four failed to produce distinct current. D112V/S143D generated small Zn^{2+}-insensitive currents that reversed at −17 ± 6.6 mV (mean ± SEM; $n = 5$) at pH_o 7.0 and pH_i 5.5, well positive to E_H, which is −87 mV. In five cells, V_{rev} shifted by −24.3 ± 1.6 mV when $CH_3SO_3^-$ was replaced with Cl^- at pH_o 5.5 and pH_i 5.5, demonstrating Cl^- permeation. That Asp at position 143 (in the S2 segment) overcame the nonconduction of D112V is consistent with position 143 facing the pore, as predicted in our model, but in a location incompatible with its producing H^+ selectivity.

MD simulations reveal significant differences in the electrostatic properties of mutant channels

To assess the structural impact of the filter shift, MD simulations were performed on the WT protein, single-point mutants D112V and D112S, and double mutants D112V/V116D (VD) and D112V/V112S (VS) in a hydrated lipid bilayer bathed in 500 mM NaCl, based on our homology model (Kulleperuma et al., 2013). The overall structure of the channel was preserved in the mutants. In particular, the average root-mean-square deviation between WT and mutants ranged from 2.0 Å

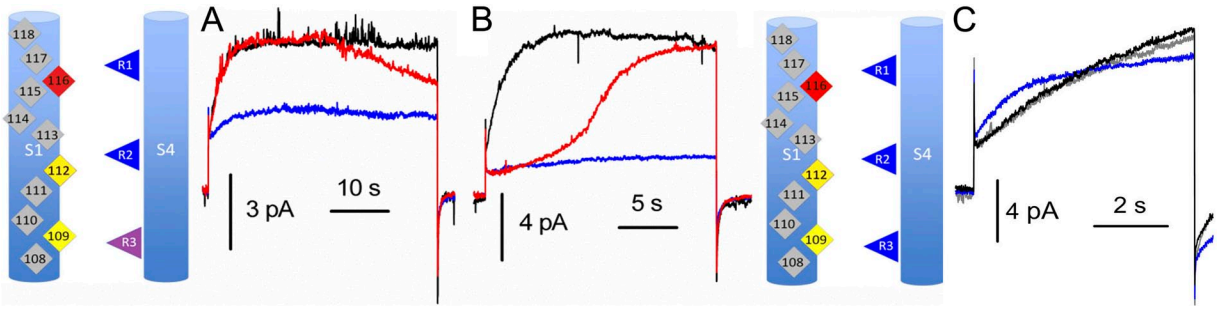

Figure 8. The third arginine position in the S4 segment is accessible to the internal solution in the open state. (A) The black trace shows proton current in D112V/V116D/R211H in an inside-out patch from a HEK-293 cell. 10 µM Zn^{2+} was introduced into the internal solution during the red trace, and blue is the subsequent pulse in the continued presence of Zn^{2+}. (B) The blue record is from D112V/V116D/R211H in the presence of 10 µM Zn^{2+}, and the red record shows recovery from block on the addition of EGTA shortly after the start of the pulse. Black represents after washout. (C) The control mutant, D112V/V116D, in a COS-7 cell exhibits weak IC Zn^{2+} sensitivity: black, before; blue, in 10 µM Zn^{2+}; gray, after washout. All pulses are to +50 mV at pH_i 7.0 and pH_o 7.0 in inside-out patches of membrane.

Published November 11, 2013

(D112S) to 2.2 Å (D112V). In all five systems, the average axial position of helices S1–S4 relative to the rest of the bundle was 0.73 ± 0.06 Å, 0.34 ± 0.05 Å, −1.80 ± 0.16 Å, and 0.53 ± 0.06 Å (SEM), respectively, indicating that the registry of the four helices was conserved in all the simulations. Combining data from the five systems leads to axial distributions that fit a single Gaussian distribution for each of the four helices, S1–S4, with standard deviations σ = 0.4, 0.5, 0.7, and 0.4 Å, respectively, emphasizing the small amplitude of axial fluctuations. Furthermore, the average hydration profiles of the pore in WT and various mutants did not differ significantly from one another (Fig. 9). The pore is characterized by an hourglass shape with an ∼13-Å-long narrow region comprising an IC bottleneck at Phe^{150} and an extracellular (EC) bottleneck at Asp^{112}. It is noteworthy that average pore hydration was quite similar for proton-selective (WT, VD), anion-permeable (VS, S = D112S), and nonconducting mutants (VAL = D112V), indicating that the mean hydration profile is not a good predictor of selectivity.

Despite these overall similarities (Fig. 9), differences were evident in the local structure of the pore near the EC bottleneck (Fig. 10). In the WT (Fig. 10 A), the EC constriction usually consists of a salt bridge between Arg^{208} and Asp^{112} (or occasionally Asp^{185}), whereas the other charged residues in the EC vestibule, namely Asp^{185} and Arg^{205}, usually form a spatially distinct ion pair. Consistent with our previous simulation study (Kulleperuma et al., 2013), Asp^{112}–Arg^{208} in WT is present as an ion pair most of the time but is occasionally disrupted by water molecules, resulting in the transient appearance of a water chain. In all four mutants considered, however, the absence of a charged side chain at position 112 led to the reorganization of the ionic network in the EC vestibule. In the proton-selective VD mutant (Fig. 10 B), various arrangements of ionic networks involving between two and four charged side chains from helices S1 (Asp^{116}), S3 (Asp^{185}), and S4 (Arg^{205} and Arg^{208}) were observed. Fig. 11 illustrates the most frequent configurations adopted by Asp^{116}. Most of the time (∼82%), it interacts with Arg^{205} (Fig. 11 A) or Arg^{208}

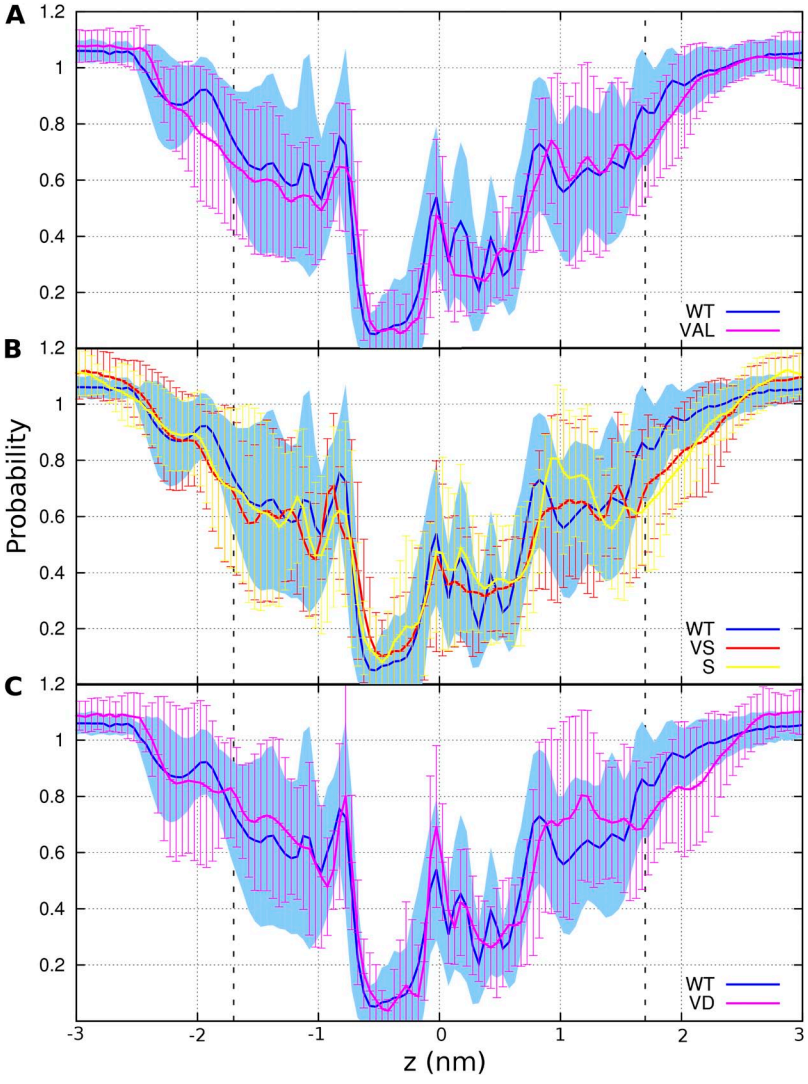

Figure 9. Pore hydration is similar in WT and several mutant channels despite very different selectivity. Average water density within a 0.7-nm radius of the mean axis of the pore is plotted, normalized to the bulk water density for 5,000 snapshots from each replica of different systems. The membrane boundaries are indicated by dashed lines, with the external surface to the right. The nadir is near Phe^{150} in all cases. Average axial water density for: (A) WT (proton selective) and D112V (VAL, nonconducting); (B) WT and D112V/V116S (VS) and D112S (S), two anion-permeable channels; (C) WT and D112V/V116D (VD), of which both are proton selective.

Published November 11, 2013

(Fig. 11 D) or both (Fig. 11 C). Similarly, in WT hH_V1, Asp^{112} was engaged in salt linkage 90% of the time but almost exclusively with Arg^{208}. However, in WT hH_V1, a continuous water chain was present only when the Asp^{112}–Arg^{208} salt bridge was broken, which occurred ~10% of the time (Kulleperuma et al., 2013). In contrast, water pathways were observed in all configurations of the VD mutant, reflecting the greater width of the pore at this level compared with position 112. That an aqueous pathway is not predictive of proton selectivity is not surprising given the example of aquaporin channels that conduct water at high rate but are impermeable to protons (Zeidel et al., 1994). In contrast with WT, pore hydration is not significantly modulated by the configurations of Asp^{116} in the VD mutant.

In particular, Arg^{208} was observed to form ion pairs with Asp^{116}, Asp^{185}, or neither, or both. In contrast to WT, the local hydration of the constriction at the bottom of the EC funnel does not depend on whether or not Arg^{208} is engaged in ion pairing (Fig. 10 B). Furthermore, our models predict the presence of water pathways in the anionic mutants D112S and VS (Fig. 10, C and D), and even in the nonconducting D112V mutant (Fig. 10 E). In all systems considered, the channel contains a narrow bottleneck ~0.5 nm in length ($-0.68 < z < -0.18$ nm) between the tips of the EC and IC funnels. Although this bottleneck is lined with nonpolar residues including Val^{109}, Phe^{150}, Val^{178}, and Val^{209}, it contains a single file of two water molecules at least 75% of the time, consistent with a putative ion pathway between the EC and IC funnels.

As a first step toward characterizing the energetics of ion permeation in the channel, we computed the static-field energy for a virtual positive point charge along water pathways spanning the length of the channel. Fig. 12 A shows that D112V, D112S, and VS mutants contain an

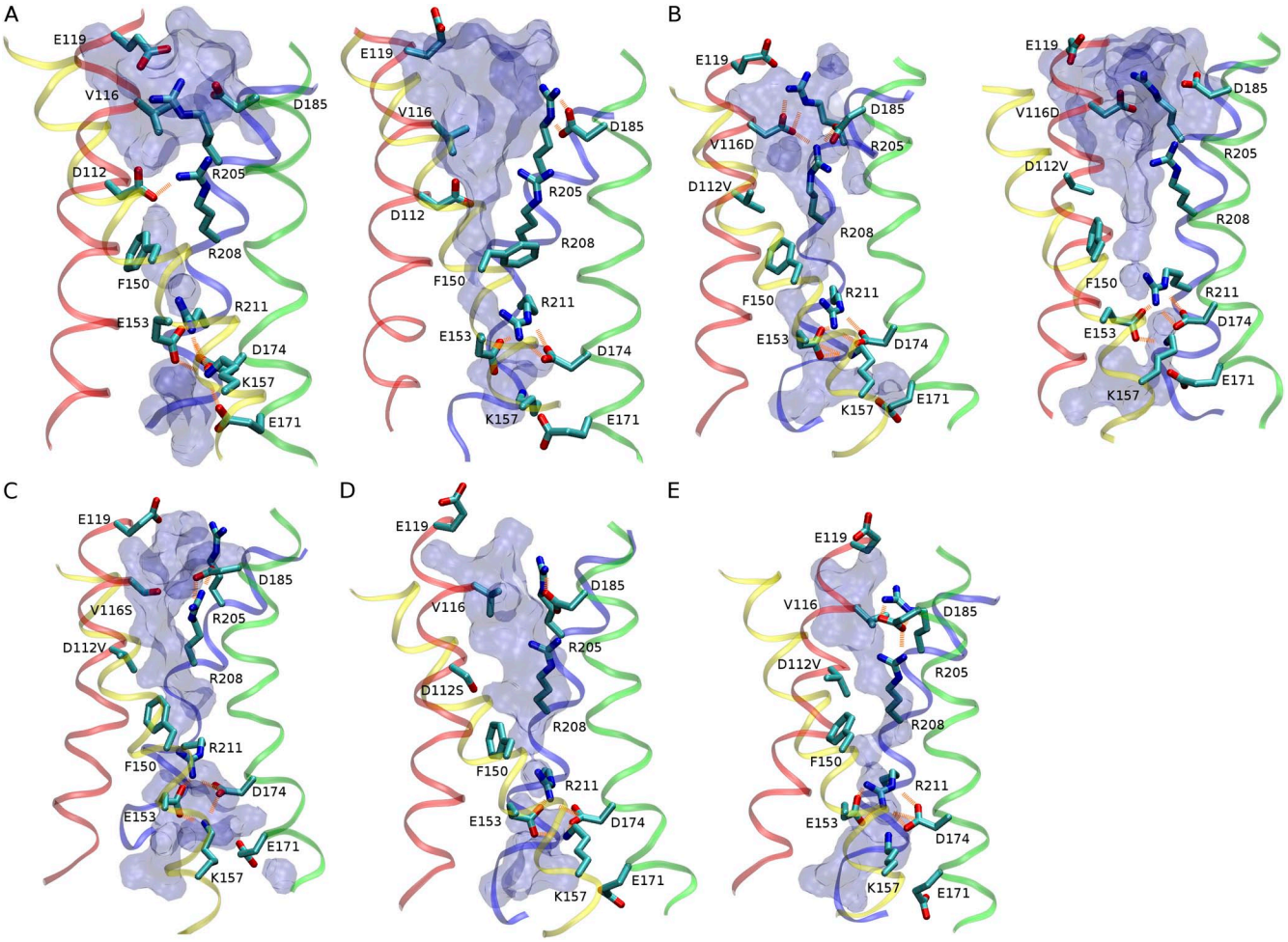

Figure 10. The EC salt-link network realigns in mutants. Representative snapshots of ionic networks in the WT and mutants, with the external end up. (A) WT protein in contact (left) and water-mediated (right) states of the D112–R208 ion pair. (B) VD mutant, with R208 participating in (left) and free from (right) the EC salt-link network. (C) VS mutant. (D) D112S mutant. (E) D112V mutant. Acidic and basic side chains in the external and internal funnel, together with side chains of residues 112, 116, F150, and R211 are shown in licorice representation together with ribbon traces of the four α-helical transmembrane regions: red, S1; yellow, S2; green, S3; blue, S4. Salt bridges are shown as orange lines. The volumetric surface of water within the pore is shown with a water radius of 0.14 nm.

Published November 11, 2013

electrostatic barrier opposing the movement of a cation through the EC side of the bottleneck, which is lacking in the WT. In contrast, the energetic properties of the VD double mutant depend on the local arrangement of ionic residues in the EC funnel. Specifically, a static-field barrier to cation movement is present at the EC bottleneck when Arg^{208} does not take part in any salt link (Fig. 12 A, "VD unpaired"), but this barrier is reduced by at least one half when the guanidinium group of Arg^{208} is paired with the carboxylate group of either Asp^{116} or Asp^{185}, or both (Fig. 12 B, "SL," salt linkage). In the latter cases, the static-field profile becomes comparable to that of WT. Intriguingly, the electrostatic profile seems to be relatively insensitive to the nature of the ionic pairing of Asp^{116} (illustrated in Fig. 11).

Collectively, the above results suggest that the lack of proton selectivity in D112V, D112S, and VS mutants is caused at least in part by the distribution of charged groups in the lumen, where the presence of an excess positive charge near the EC constriction would tend to favor anions over cations. This finding is consistent with the anionic selectivity of D112S and VS mutants. Inversely, the neutrality of the EC bottleneck region in WT and VD systems results in approximate cancellation of the static field, which, although it does not explain proton selectivity, is consistent with the fact that these two channels are permeable to a cation.

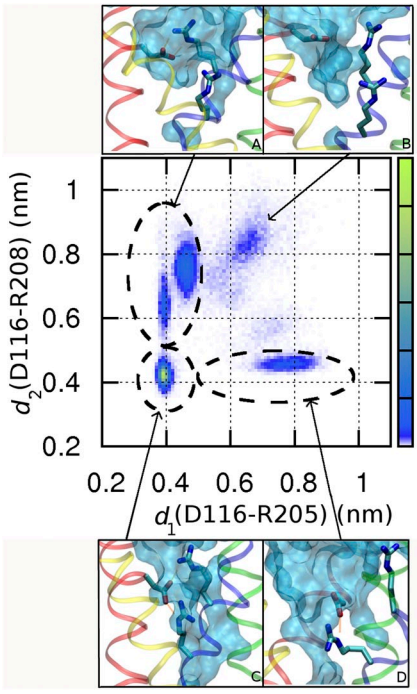

Figure 11. Several configurations of Asp^{116} in the D112V/V116D mutant. Two-dimensional histogram of the distances from the center of charge of D116 to that of R205 (d_1) and R208 (d_2), respectively, with increasing probability of ion pairing from purple to green. Snapshots surrounding the graph illustrate each type of interaction circled in the graph: (A) linked D116–R205 pair, 37% of the time; (B) open (no salt bridge), 18%; (C) D116 linked to R205 and R208 simultaneously, 33%; (D) D116–R208 salt bridge, 12%.

DISCUSSION

Nonconducting mutants

When the critical Asp^{112} residue was moved along the S1 segment from position 108 through 118 (with D112A), 8 of 10 mutants did not conduct, proton current was seen at 116, and anion current was seen at 109. Positions 116, 112, and 109 all face the "pore" in the predicted open-state structure of hH_V1 (Kulleperuma et al., 2013). Asp at pore-facing position 143 in the S2 segment also exhibited anion current. Evidently, the Asp carboxyl group must face the pore to enable conductance of any kind, and with Asp at a nonpore-facing location, the S1 segment is not free to rotate enough for the carboxyl group to reach the pore. When Asp faces away from the pore, its pK_a likely increases substantially, making it permanently neutral. When Lys was introduced at a series of locations in the acetylcholine receptor channel, its pK_a was decreased, often drastically, when it did not face the pore directly (Cymes et al., 2005). When ionizable amino acids are inserted inside proteins by mutation, their pK_a generally shifts in the direction that promotes neutrality (Isom et al., 2008). In contrast, in native proteins, ionizable residues have evolved to establish interactions with their neighbors that favor ionization (Kim et al., 2005; Gunner et al., 2011).

The rules of the game

The selectivity of various mutants summarized in Table 1 reveals "the rules of the game" for hH_V1. In the mutants studied, the presence of Asp or Glu at position 112 or 116 was necessary and sufficient to produce H^+ selectivity. The identity of the amino acid at position 109 had no effect; selectivity was determined entirely by positions 112 and 116. When Val was present at both critical positions, 112 and 116, the channel failed to conduct (an effect that was not overcome by introducing Asp at 109). That Val seems to disfavor permeation may reflect its relative hydrophobicity (Kyte and Doolittle, 1982; Hessa et al., 2005). The VxxDxxxV motif (or a closely conserved version in which Leu replaces Val^{109} and/or Val^{116}) appears in the S1 segment of all eight species with electrophysiologically confirmed H_V1 (DeCoursey, 2013). In hHv1, when positions 112 and 116 were occupied by Val and a small neutral amino acid (Ala or Ser, for example) in either order, the result was anion permeation.

Microenvironment of positions 112 and 116

With respect to selectivity, voltage dependence, kinetics, and ΔpH dependence of gating, the filter-shifted D112V/V116D channels were quite similar to WT. In

Published November 11, 2013

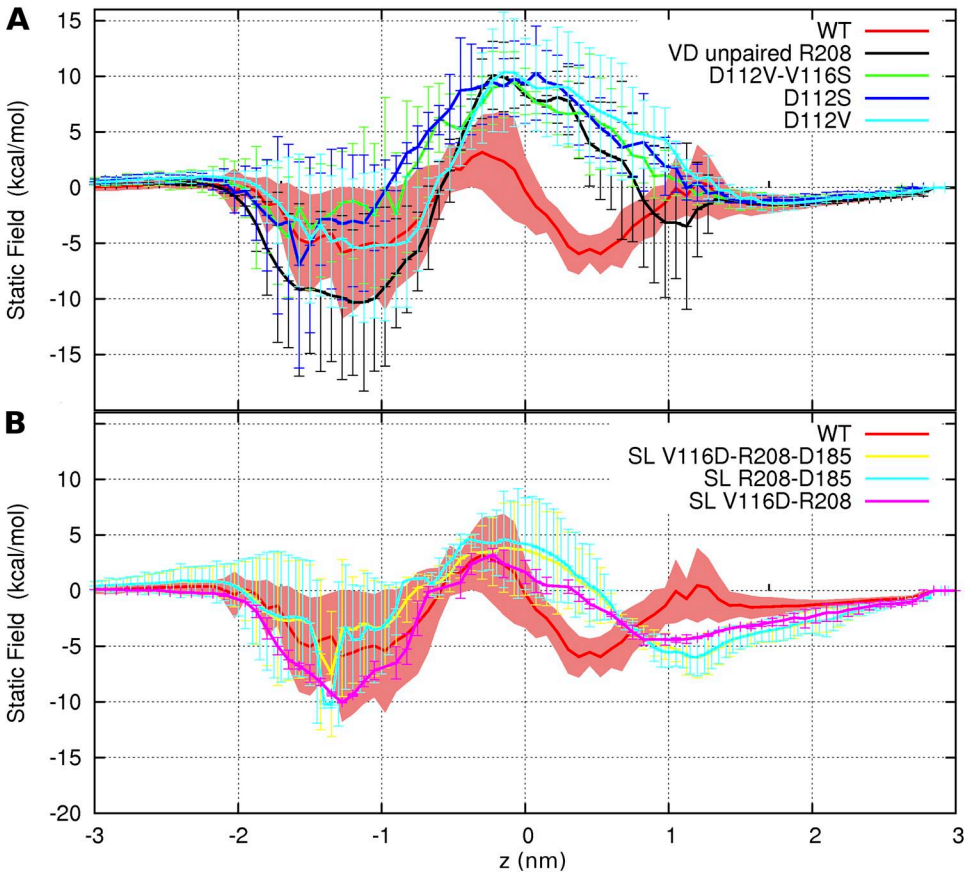

Figure 12. Effect of the charge distribution of the channel on the energetics of ion translocation in WT and mutant channels. Orientation is as in Fig. 9, with the external solution to the right. Static-field energy for the transfer of a positive point charge in (A) WT, D112V, VD when R208 is unbound to the EC salt-link network, and two anion-permeable channels, VS and D112S. (B) WT and VD when R208 is forming salt link(s) (SL) with V116D or D185, or both.

addition, the effects of point mutations at position 116 closely resembled those at 112. Glu replacing Asp at either position preserves proton specificity. Channels with neutral residues like Ser or Asn at either position (with Val occupying the other) conduct anions. These phenomenological parallels indicate that in terms of the molecular details required to establish proton (or anion) selectivity, the two positions are virtually indistinguishable. However, the identities of individual neighbors of the critical aspartate differ substantially at the two positions. Side chains with atoms within 6 Å of Asp^{112} (WT) or Asp^{116} (in the D112V background) at least 50% of the time were identified from time-averaging of MD simulations. Intriguingly, in WT, the nearest neighbors to Asp^{112}, excluding those on the S1 segment (Ala^{113}, Leu^{111}, Leu^{115}, Val^{116}, and Val^{109}), include residues on both S2 (Ile^{146}, Ser^{143}, and Phe^{150}) and S4 (Arg^{208}), whereas in the VD mutant, only S4 residues (Arg^{205} and Arg^{208}; along with S1 residues Leu^{117}, Glu^{119}, Leu^{115}, and Leu^{120}) are within 6 Å of Asp^{116}. In the D112V/V116D

TABLE 1

Effects on selectivity of amino acids at positions 109, 112, and 116 in the S1 transmembrane segment of hH_V1

Construct	109	112	116	Selectivity	Reference
WT hH_V1	Val	**Asp**	Val	H^+	Many
A113D	Val	**Asp**	Val	H^+	This
D112E	Val	**Glu**	Val	H^+	Musset et al., 2011
D112A/V116D	Val	*Ala*	**Asp**	H^+	This
D112V/V116D	Val	Val	**Asp**	H^+	This
D112V/V116E	Val	Val	**Glu**	H^+	This
D112V	Val	Val	Val	0	Musset et al., 2011
D112V/V109D	**Asp**	Val	Val	0	This
D112A, N, S, H, K, F	Val	*Ala*	Val	Cl^-	Musset et al., 2011
D112A/V109D	**Asp**	*Ala*	Val	Cl^-	This
D112V/V116S	Val	Val	*Ser*	Cl^-	This
D112V/V116N	Val	Val	*Asn*	Cl^-	This

Selectivity to H^+ means V_{rev} was close to E_H at various ΔpH; 0 means no credible currents; Cl^- means V_{rev} shifted negatively when Cl^- replaced $CH_3SO_3^-$ in the external solution. Acidic residues are bold; neutral residues other than Val are italicized.

Published November 11, 2013

mutant, the selectivity filter is roughly twice as far from Phe^{150} (the external delimiter of the charge transfer center; Tao et al., 2010) as Asp^{112} is in the WT channel. This result means that immediate proximity of the carboxyl group to the most hydrophobic point in the channel, which in all constructs occurs at Phe^{150} (Figs. 9 and 10), is not essential to establishing any of the main features of the channel, including proton specificity, gating kinetics, and ΔpH-dependent gating.

Why does 109 not work?

The lack of influence of position 109 (Table 1) suggests that selectivity is established in the external vestibule, outside the charge transfer center boundary at Phe^{150}. All current models of hH_V1 place Asp^{112} in the external vestibule (Musset et al., 2010; Ramsey et al., 2010; Wood et al., 2012; Kulleperuma et al., 2013). The MD simulations provide additional insight. In WT hH_V1, Asp^{112} is frequently paired with Arg^{208}. During the 10% of the time that these residues were unpaired, a continuous water wire was present. With Asp moved to 116, there was an electrostatic barrier to cation permeation when Arg^{208} was unpaired, but not when it was paired with either Asp^{185} or Asp^{116}. In support of these findings, an unpaired Arg residue near the EC mouth of aquaporin channels is essential to block the translocation of protons (Beitz et al., 2006; Wu et al., 2009).

Limited plasticity of the channel with respect to axial helix movement does not support a change of S1 registry in the mutants

The interpretation of measurable effects of point mutations assumes conservation of the global protein conformation. Accordingly, we have modeled the structure of the mutants by substituting individual side chains in our model of the WT. An alternative interpretation for the native-like phenotype of the VD double mutant is that the S1 helix is shifted by one turn toward the interior of the cell, so that D112V and V116D take the place of V109 and D112, respectively. However, the analysis of collective fluctuations from the simulations shows that not only were the overall structure and hydration of the channel conserved, but there was also no significant axial displacement of individual helices in response to any of the mutations, and the plasticity of the channel with respect to axial helix movement remained limited in all the systems studied (Figs. S1 and S2). Although the possibility of a change in S1 registry with respect to the rest of the bundle cannot be ruled out, these results suggest that such a change is unlikely in any of the mutants considered in the present study.

Collectively, our current findings suggest that charge neutrality resulting from the presence of Asp (or Glu) vis-à-vis Arg^{208} at the external constriction is required for the charge selectivity of the channel; in particular, the presence of an excess positive charge at the narrow end of the external funnel in neutral Asp^{112} mutants leads to a barrier opposing cation movement but compatible with anion selectivity. In addition, the presence of an ionic network involving Arg^{208} results in dynamic fluctuations of pore hydration and/or electrostatic properties that may contribute to the mechanism of proton selectivity in the WT and VD channels.

Parallels in other molecules

To our knowledge, hH_V1 is the first example of a selective ion channel whose selectivity filter can be moved by a pair of point mutations. The acetylcholine receptor channel remains nonselective among cations when its ring of Glu residues is shifted by one turn of the α helix (Cymes and Grosman, 2012). Several other proton-conducting pathways permit shifts of critical amino acids, although in these molecules the portable function is primarily rapid proton flux rather than proton selectivity per se. For example, in F_1F_o-type ATP synthase (*Escherichia coli*), proton translocation is preserved when Asp^{61} is shifted to position 24 on another helix (Miller et al., 1990). Asp^{61} can be replaced by Glu^{61}, but with diminished proton transport, suggesting that precise location of the carboxyl is critical (Fillingame, 1990). Portability of Asp shows that the precise structure of apolar neighbors of the carboxyl group is not critical (Fillingame, 1990). Another essential residue in ATP synthase is Arg^{210}, which is thought to lower the pK_a of Asp^{61} transiently to ensure proton release (Fillingame et al., 2003; von Ballmoos et al., 2009).

As in ATP synthase, an Asp^{213} critical for proton translocation in nicotinamide nucleotide transhydrogenase can be replaced by Glu, but activity is decreased to 18% (Yamaguchi et al., 2002). In enzyme studies, activity that is rate-limited by proton translocation is assessed. The correlate in hH_V1 is single-channel conductance, which was not examined here. Our criterion is perfect proton selectivity, which is preserved when Glu replaces Asp at either position 112 or 116 in hH_V1. We cannot say whether Glu is equally efficient.

When Asp^{135} in the proton entry channel in cytochrome bo_3 ubiquinol oxidase of *E. coli* is neutralized, its function can be restored by shifting Asp to position 139 or 142 (Garcia-Horsman et al., 1995).

Neutralizing Asp^{132}, the namesake of the D channel in cytochrome *c* oxidase from *Rhodobacter sphaeroides*, by mutations D132N or D132A nearly abolishes proton uptake (Fetter et al., 1995), which is restored by repositioning the Asp at N139D (Varanasi and Hosler, 2011, 2012). Intriguingly, proton uptake is also restored by removing subunit III (Ädelroth and Hosler, 2006) and also in the D132N/N139T double mutant, showing that in the D channel, rapid proton uptake can be accomplished without an acidic group, although enzyme turnover remains impaired (Johansson et al., 2013). Asn^{139} is thought to serve a special "gating" function in cytochrome

c oxidase that may normally limit WT H^+ flux (Henry et al., 2009); Thr^{139} appears to optimize aqueous connectivity within the pore (Johansson et al., 2013).

Finally, His^{64} shuttles protons from the catalytic center of human carbonic anhydrase II, and function is preserved with His shifted to His^{67} (H64A/N67H), but not His^{62} (H64A/N62H), despite crystal structures indicating that the side chains of both His^{62} and His^{67} extend into the active-site cavity at distances from the catalytic zinc similar to His^{64} (Fisher et al., 2005).

These examples show that an amino acid side chain must be positioned correctly to maintain a high rate of proton transfer, but that in some cases a reasonable rate of proton transfer can be retained upon moving the side chain, especially if it is not moved too far. Given that proton transfer via titratable amino acid side chains is a way to achieve proton selectivity, proton transfer and proton selectivity may be the same process, and thus in some cases, a side chain essential for H^+ selectivity may be moved without losing selectivity.

In summary, shifting Asp along the S1 segment identified three locations in hH_V1 that line the pore and permit conduction: 109, 112, and 116. Asp produced proton specificity only at positions 112 and 116. When introduced at nonpore-facing positions, Asp abolished function. Glu at either position preserved selectivity, indicating leeway in side-chain length. We conclude that the minimal requirements for proton specificity of hH_V1 include Asp or Glu, which must face the pore directly, and evidently must be located in the external vestibule, above the charge transfer center, Phe^{150}. The portability of the selectivity filter indicates latitude in the requisite local environment. This observation seems consistent with the suggestion that ionizable groups that enable proton transport could have evolved by random mutation without the need to simultaneously develop a specialized microenvironment for charge stabilization (Isom et al., 2008). On the other hand, the inability of Asp to produce H^+-selective conductance at most positions tested argues that additional factors are involved. Modeling indicates frequent salt-bridge formation between Asp and several partners, which may contribute to selectivity, proton transfer, and conformational stability. Ionizable residues favor the incorporation of water molecules (Pless et al., 2011) that may also facilitate proton translocation. However, neither the presence of a continuous water pathway nor the mean hydration profile was found to have any clear relationship with the selectivity of the channel. Detailed computational studies of H^+ and other ions in the permeation pathway will be required to examine the molecular basis of ion movement and achieve a full understanding of the mechanism of proton selectivity in hHv1.

The authors appreciate helpful discussions with Jonathan Hosler.

Supported by National Science Foundation award MCB-0943362 to T.E. DeCoursey and S.M.E. Smith; Canadian Institutes of Health Research operating grants MOP43949 and MOP130461 to R. Pomès; and National Institutes of Health (NIH) grant R01-GM087507 to T.E. DeCoursey. The content is solely the responsibility of the authors and does not necessarily represent the official views of the NIH. Computations were performed on the GPC supercomputer at the SciNet HPC Consortium. SciNet is funded by the Canada Foundation for Innovation under the auspices of Compute Canada, the Government of Ontario, the Ontario Research Fund, and the University of Toronto.

Kenton J. Swartz served as editor.

Submitted: 10 June 2013
Accepted: 17 October 2013

REFERENCES

Ädelroth, P., and J. Hosler. 2006. Surface proton donors for the D-pathway of cytochrome *c* oxidase in the absence of subunit III. *Biochemistry.* 45:8308–8318. http://dx.doi.org/10.1021/bi0605843

Beitz, E., B. Wu, L.M. Holm, J.E. Schultz, and T. Zeuthen. 2006. Point mutations in the aromatic/arginine region in aquaporin 1 allow passage of urea, glycerol, ammonia, and protons. *Proc. Natl. Acad. Sci. USA.* 103:269–274. http://dx.doi.org/10.1073/pnas.0507225103

Berger, O., O. Edholm, and F. Jähnig. 1997. Molecular dynamics simulations of a fluid bilayer of dipalmitoylphosphatidylcholine at full hydration, constant pressure, and constant temperature. *Biophys. J.* 72:2002–2013. http://dx.doi.org/10.1016/S0006-3495(97)78845-3

Capasso, M., M.K. Bhamrah, T. Henley, R.S. Boyd, C. Langlais, K. Cain, D. Dinsdale, K. Pulford, M. Khan, B. Musset, et al. 2010. HVCN1 modulates BCR signal strength via regulation of BCR-dependent generation of reactive oxygen species. *Nat. Immunol.* 11:265–272. http://dx.doi.org/10.1038/ni.1843

Chakrabarti, N., C. Neale, J. Payandeh, E.F. Pai, and R. Pomès. 2010. An iris-like mechanism of pore dilation in the CorA magnesium transport system. *Biophys. J.* 98:784–792. http://dx.doi.org/10.1016/j.bpj.2009.11.009

Cherny, V.V., and T.E. DeCoursey. 1999. pH-dependent inhibition of voltage-gated H^+ currents in rat alveolar epithelial cells by Zn^{2+} and other divalent cations. *J. Gen. Physiol.* 114:819–838. http://dx.doi.org/10.1085/jgp.114.6.819

Cherny, V.V., V.S. Markin, and T.E. DeCoursey. 1995. The voltage-activated hydrogen ion conductance in rat alveolar epithelial cells is determined by the pH gradient. *J. Gen. Physiol.* 105:861–896. http://dx.doi.org/10.1085/jgp.105.6.861

Cherny, V.V., R. Murphy, V. Sokolov, R.A. Levis, and T.E. DeCoursey. 2003. Properties of single voltage-gated proton channels in human eosinophils estimated by noise analysis and by direct measurement. *J. Gen. Physiol.* 121:615–628. http://dx.doi.org/10.1085/jgp.200308813

Cymes, G.D., and C. Grosman. 2012. The unanticipated complexity of the selectivity-filter glutamates of nicotinic receptors. *Nat. Chem. Biol.* 8:975–981. http://dx.doi.org/10.1038/nchembio.1092

Cymes, G.D., Y. Ni, and C. Grosman. 2005. Probing ion-channel pores one proton at a time. *Nature.* 438:975–980. http://dx.doi.org/10.1038/nature04293

DeCoursey, T.E. 2010. Voltage-gated proton channels find their dream job managing the respiratory burst in phagocytes. *Physiology (Bethesda).* 25:27–40. http://dx.doi.org/10.1152/physiol.00039.2009

DeCoursey, T.E. 2013. Voltage-gated proton channels: molecular biology, physiology, and pathophysiology of the H_V family. *Physiol. Rev.* 93:599–652. http://dx.doi.org/10.1152/physrev.00011.2012

DeCoursey, T.E., D. Morgan, and V.V. Cherny. 2003. The voltage dependence of NADPH oxidase reveals why phagocytes need

proton channels. *Nature.* 422:531–534. http://dx.doi.org/10.1038/nature01523

Demaurex, N. 2012. Functions of proton channels in phagocytes. *Wiley Interdiscip. Rev. Membr. Transp. Signal.* 1:3–15. http://dx.doi.org/10.1002/wmts.2

Fetter, J.R., J. Qian, J. Shapleigh, J.W. Thomas, A. García-Horsman, E. Schmidt, J. Hosler, G.T. Babcock, R.B. Gennis, and S. Ferguson-Miller. 1995. Possible proton relay pathways in cytochrome *c* oxidase. *Proc. Natl. Acad. Sci. USA.* 92:1604–1608. http://dx.doi.org/10.1073/pnas.92.5.1604

Fillingame, R.H. 1990. Molecular mechanics of ATP synthesis by F_1F_0–type H^+-transporting ATP synthases. *In* The Bacteria. Volume 12. T.A. Krulwich, editor. Academic Press, New York. 345–390.

Fillingame, R.H., C.M. Angevine, and O.Y. Dmitriev. 2003. Mechanics of coupling proton movements to *c*-ring rotation in ATP synthase. *FEBS Lett.* 555:29–34. http://dx.doi.org/10.1016/S0014-5793(03)01101-3

Fischer, H. 2012. Function of proton channels in lung epithelia. *Wiley Interdiscip Rev Membr Transp Signal.* 1:247–258. http://dx.doi.org/10.1002/wmts.17

Fisher, Z., J.A. Hernandez Prada, C. Tu, D. Duda, C. Yoshioka, H. An, L. Govindasamy, D.N. Silverman, and R. McKenna. 2005. Structural and kinetic characterization of active-site histidine as a proton shuttle in catalysis by human carbonic anhydrase II. *Biochemistry.* 44:1097–1105. http://dx.doi.org/10.1021/bi0480279

Garcia-Horsman, J.A., A. Puustinen, R.B. Gennis, and M. Wikström. 1995. Proton transfer in cytochrome bo_3 ubiquinol oxidase of *Escherichia coli*: second-site mutations in subunit I that restore proton pumping in the mutant Asp135→Asn. *Biochemistry.* 34:4428–4433. http://dx.doi.org/10.1021/bi00013a035

Gonzalez, C., H.P. Koch, B.M. Drum, and H.P. Larsson. 2010. Strong cooperativity between subunits in voltage-gated proton channels. *Nat. Struct. Mol. Biol.* 17:51–56. http://dx.doi.org/10.1038/nsmb.1739

Gunner, M.R., X. Zhu, and M.C. Klein. 2011. MCCE analysis of the pK_as of introduced buried acids and bases in staphylococcal nuclease. *Proteins.* 79:3306–3319. http://dx.doi.org/10.1002/prot.23124

Henderson, L.M., J.B. Chappell, and O.T.G. Jones. 1988. Superoxide generation by the electrogenic NADPH oxidase of human neutrophils is limited by the movement of a compensating charge. *Biochem. J.* 255:285–290.

Henry, R.M., C.H. Yu, T. Rodinger, and R. Pomès. 2009. Functional hydration and conformational gating of proton uptake in cytochrome *c* oxidase. *J. Mol. Biol.* 387:1165–1185. http://dx.doi.org/10.1016/j.jmb.2009.02.042

Hessa, T., H. Kim, K. Bihlmaier, C. Lundin, J. Boekel, H. Andersson, I. Nilsson, S.H. White, and G. von Heijne. 2005. Recognition of transmembrane helices by the endoplasmic reticulum translocon. *Nature.* 433:377–381. http://dx.doi.org/10.1038/nature03216

Humphrey, W., A. Dalke, and K. Schulten. 1996. VMD: visual molecular dynamics. *J. Mol. Graph.* 14:33–38. http://dx.doi.org/10.1016/0263-7855(96)00018-5

Isom, D.G., B.R. Cannon, C.A. Castañeda, A. Robinson, and B. García-Moreno. 2008. High tolerance for ionizable residues in the hydrophobic interior of proteins. *Proc. Natl. Acad. Sci. USA.* 105:17784–17788. http://dx.doi.org/10.1073/pnas.0805113105

Johansson, A.L., M. Högbom, J. Carlsson, R.B. Gennis, and P. Brzezinski. 2013. Role of aspartate 132 at the orifice of a proton pathway in cytochrome *c* oxidase. *Proc. Natl. Acad. Sci. USA.* 110:8912–8917. http://dx.doi.org/10.1073/pnas.1303954110

Jorgensen, W.L., J. Chandrasekhar, J.D. Madura, R.W. Impey, and M.L. Klein. 1983. Comparison of simple potential functions for simulating liquid water. *J. Chem. Phys.* 79:926–935. http://dx.doi.org/10.1063/1.445869

Jorgensen, W.L., D.S. Maxwell, and J. Tirado-Rives. 1996. Development and testing of the OPLS all-atom force-field on conformational energetic and properties of organic liquids. *J. Am. Chem. Soc.* 118:11225–11236. http://dx.doi.org/10.1021/ja9621760

Kandt, C., W.L. Ash, and D.P. Tieleman. 2007. Setting up and running molecular dynamics simulations of membrane proteins. *Methods.* 41:475–488. http://dx.doi.org/10.1016/j.ymeth.2006.08.006

Kim, J., J. Mao, and M.R. Gunner. 2005. Are acidic and basic groups in buried proteins predicted to be ionized? *J. Mol. Biol.* 348:1283–1298. http://dx.doi.org/10.1016/j.jmb.2005.03.051

Kulleperuma, K., S.M.E. Smith, D. Morgan, B. Musset, J. Holyoake, N. Chakrabarti, V.V. Cherny, T.E. DeCoursey, and R. Pomès. 2013. Construction and validation of a homology model of the human voltage-gated proton channel hH_V1. *J. Gen. Physiol.* 141:445–465. http://dx.doi.org/10.1085/jgp.201210856

Kyte, J., and R.F. Doolittle. 1982. A simple method for displaying the hydropathic character of a protein. *J. Mol. Biol.* 157:105–132. http://dx.doi.org/10.1016/0022-2836(82)90515-0

Lishko, P.V., I.L. Botchkina, A. Fedorenko, and Y. Kirichok. 2010. Acid extrusion from human spermatozoa is mediated by flagellar voltage-gated proton channel. *Cell.* 140:327–337. http://dx.doi.org/10.1016/j.cell.2009.12.053

Miller, M.J., M. Oldenburg, and R.H. Fillingame. 1990. The essential carboxyl group in subunit c of the F_1F_0 ATP synthase can be moved and H^+-translocating function retained. *Proc. Natl. Acad. Sci. USA.* 87:4900–4904. http://dx.doi.org/10.1073/pnas.87.13.4900

Morgan, D., and T.E. DeCoursey. 2007. Analysis of electrophysiological properties and responses of neutrophils. *Methods Mol. Biol.* 412:139–175. http://dx.doi.org/10.1007/978-1-59745-467-4_11

Morgan, D., M. Capasso, B. Musset, V.V. Cherny, E. Ríos, M.J.S. Dyer, and T.E. DeCoursey. 2009. Voltage-gated proton channels maintain pH in human neutrophils during phagocytosis. *Proc. Natl. Acad. Sci. USA.* 106:18022–18027. http://dx.doi.org/10.1073/pnas.0905565106

Musset, B., V.V. Cherny, D. Morgan, Y. Okamura, I.S. Ramsey, D.E. Clapham, and T.E. DeCoursey. 2008a. Detailed comparison of expressed and native voltage-gated proton channel currents. *J. Physiol.* 586:2477–2486. http://dx.doi.org/10.1113/jphysiol.2007.149427

Musset, B., D. Morgan, V.V. Cherny, D.W. MacGlashan Jr., L.L. Thomas, E. Ríos, and T.E. DeCoursey. 2008b. A pH-stabilizing role of voltage-gated proton channels in IgE-mediated activation of human basophils. *Proc. Natl. Acad. Sci. USA.* 105:11020–11025. http://dx.doi.org/10.1073/pnas.0800886105

Musset, B., S.M. Smith, S. Rajan, V.V. Cherny, S. Sujai, D. Morgan, and T.E. DeCoursey. 2010. Zinc inhibition of monomeric and dimeric proton channels suggests cooperative gating. *J. Physiol.* 588:1435–1449. http://dx.doi.org/10.1113/jphysiol.2010.188318

Musset, B., S.M.E. Smith, S. Rajan, D. Morgan, V.V. Cherny, and T.E. DeCoursey. 2011. Aspartate 112 is the selectivity filter of the human voltage-gated proton channel. *Nature.* 480:273–277. http://dx.doi.org/10.1038/nature10557

Musset, B., R.A. Clark, T.E. DeCoursey, G.L. Petheo, M. Geiszt, Y. Chen, J.E. Cornell, C.A. Eddy, R.G. Brzyski, and A. El Jamali. 2012. NOX5 in human spermatozoa: expression, function, and regulation. *J. Biol. Chem.* 287:9376–9388. http://dx.doi.org/10.1074/jbc.M111.314955

Pless, S.A., J.D. Galpin, A.P. Niciforovic, and C.A. Ahern. 2011. Contributions of counter-charge in a potassium channel voltage-sensor domain. *Nat. Chem. Biol.* 7:617–623. http://dx.doi.org/10.1038/nchembio.622

Ramsey, I.S., M.M. Moran, J.A. Chong, and D.E. Clapham. 2006. A voltage-gated proton-selective channel lacking the pore domain. *Nature.* 440:1213–1216. http://dx.doi.org/10.1038/nature04700

Ramsey, I.S., Y. Mokrab, I. Carvacho, Z.A. Sands, M.S.P. Sansom, and D.E. Clapham. 2010. An aqueous H^+ permeation pathway

in the voltage-gated proton channel Hv1. *Nat. Struct. Mol. Biol.* 17:869–875. http://dx.doi.org/10.1038/nsmb.1826

Smith, S.M.E., D. Morgan, B. Musset, V.V. Cherny, A.R. Place, J.W. Hastings, and T.E. DeCoursey. 2011. Voltage-gated proton channel in a dinoflagellate. *Proc. Natl. Acad. Sci. USA.* 108:18162–18167. http://dx.doi.org/10.1073/pnas.1115405108

Tao, X., A. Lee, W. Limapichat, D.A. Dougherty, and R. MacKinnon. 2010. A gating charge transfer center in voltage sensors. *Science.* 328:67–73. http://dx.doi.org/10.1126/science.1185954

Varanasi, L., and J. Hosler. 2011. Alternative initial proton acceptors for the D pathway of *Rhodobacter sphaeroides* cytochrome *c* oxidase. *Biochemistry.* 50:2820–2828. http://dx.doi.org/10.1021/bi102002v

Varanasi, L., and J.P. Hosler. 2012. Subunit III-depleted cytochrome *c* oxidase provides insight into the process of proton uptake by proteins. *Biochim. Biophys. Acta.* 1817:545–551. http://dx.doi.org/10.1016/j.bbabio.2011.10.001

von Ballmoos, C., A. Wiedenmann, and P. Dimroth. 2009. Essentials for ATP synthesis by F_1F_0 ATP synthases. *Annu. Rev. Biochem.* 78:649–672. http://dx.doi.org/10.1146/annurev.biochem.78.081307.104803

Wang, Y., S.J. Li, X. Wu, Y. Che, and Q. Li. 2012. Clinicopathological and biological significance of human voltage-gated proton channel Hv1 protein overexpression in breast cancer. *J. Biol. Chem.* 287:13877–13888. http://dx.doi.org/10.1074/jbc.M112.345280

Wood, M.L., E.V. Schow, J.A. Freites, S.H. White, F. Tombola, and D.J. Tobias. 2012. Water wires in atomistic models of the Hv1 proton channel. *Biochim. Biophys. Acta.* 1818:286–293. http://dx.doi.org/10.1016/j.bbamem.2011.07.045

Wu, B., C. Steinbronn, M. Alsterfjord, T. Zeuthen, and E. Beitz. 2009. Concerted action of two cation filters in the aquaporin water channel. *EMBO J.* 28:2188–2194. http://dx.doi.org/10.1038/emboj.2009.182

Wu, L.J., G. Wu, M.R. Akhavan Sharif, A. Baker, Y. Jia, F.H. Fahey, H.R. Luo, E.P. Feener, and D.E. Clapham. 2012. The voltage-gated proton channel Hv1 enhances brain damage from ischemic stroke. *Nat. Neurosci.* 15:565–573. http://dx.doi.org/10.1038/nn.3059

Yamaguchi, M., C.D. Stout, and Y. Hatefi. 2002. The proton channel of the energy-transducing nicotinamide nucleotide transhydrogenase of *Escherichia coli*. *J. Biol. Chem.* 277:33670–33675. http://dx.doi.org/10.1074/jbc.M204170200

Zeidel, M.L., S. Nielsen, B.L. Smith, S.V. Ambudkar, A.B. Maunsbach, and P. Agre. 1994. Ultrastructure, pharmacologic inhibition, and transport selectivity of aquaporin channel-forming integral protein in proteoliposomes. *Biochemistry.* 33:1606–1615. http://dx.doi.org/10.1021/bi00172a042

Morgan et al., http://www.jgp.org/cgi/content/full/jgp.201311045/DC1

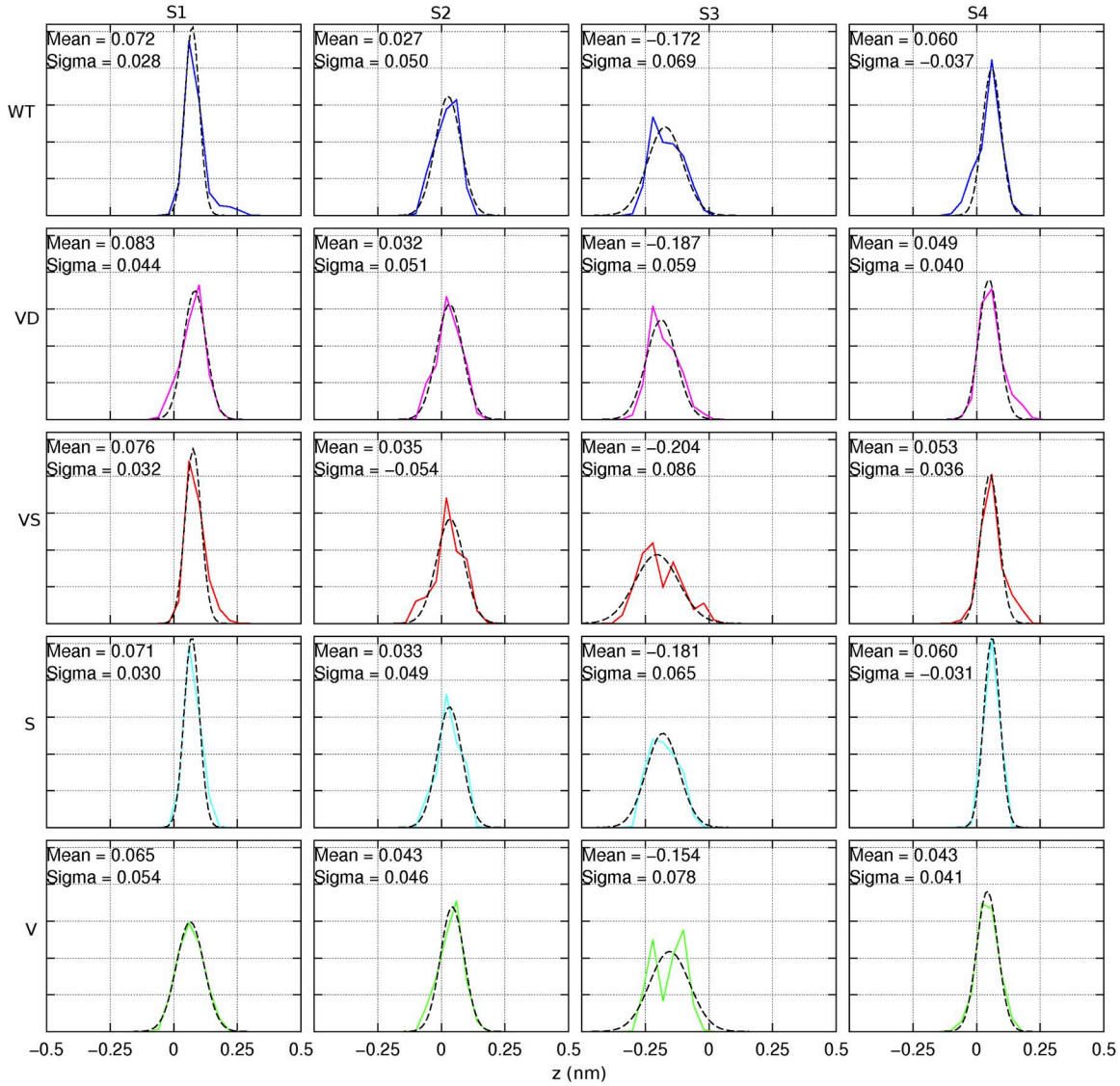

Figure S1. Axial distribution of each of the four helical segments, S1–S4, in each of the five systems (WT, VD, VS, D112V, and D112S) accumulated from the MD simulations in a lipid bilayer (solid line). Gaussian fits are also shown (dashed lines) for each of the curves. The five systems retained highly similar helical arrangements, with only small deviations in the average position of each helix relative to the rest of the protein. In all five systems, the average position of helix S1 was 0.73 ± 0.06 Å (SEM between the five systems), whereas helices S2, S3, and S4 were located at 0.34 ± 0.05 Å, −1.80 ± 0.16 Å, and 0.53 ± 0.06 Å, respectively. In other words, the registry of the four helices relative to one another was identical throughout the simulations of all five systems.

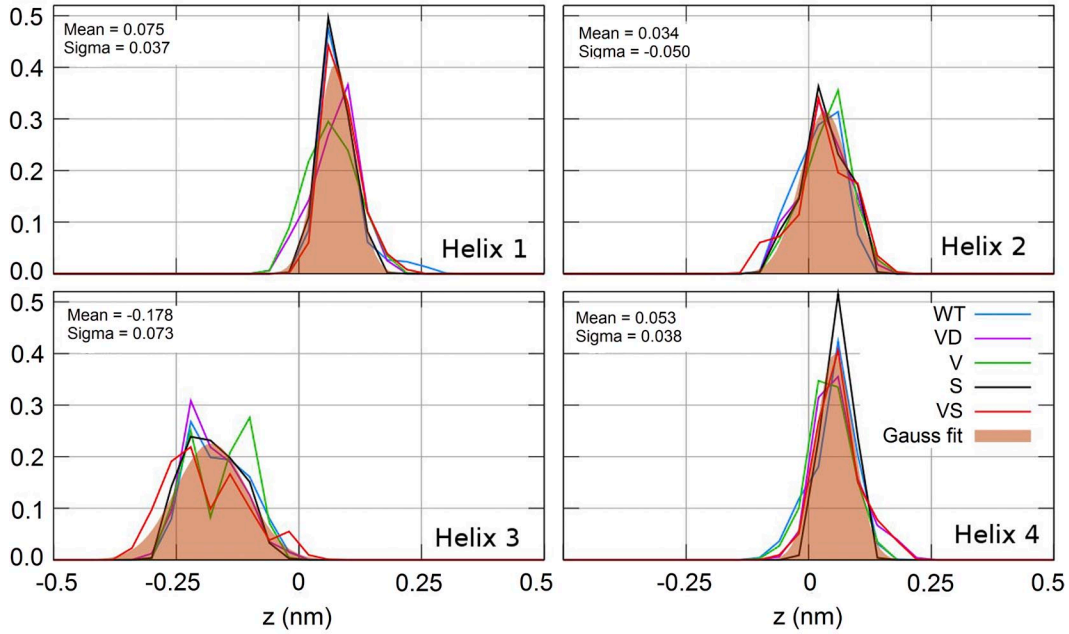

Figure S2. Axial distribution of S1–S4 from the five systems (colored lines) are superimposed, and a unique Gaussian fit is obtained for the combined data for each helix (salmon surface). The distribution of S1 fits a Gaussian distribution at 0.75 Å (standard deviation σ = 0.4 Å). Likewise, the fits for helices S2, S3, and S4 were 0.3 (σ = 0.5), −1.8 (σ = 0.7), and 0.5 (σ = 0.4) Å, respectively. The results emphasize the small amplitude of the axial fluctuations and show that S1 does not exhibit significant plasticity in the axial direction.

Table S1
Impermeability of D112V/V116D and D112V/V116D/R211H channels to ions

Construct	Ion	V_{rev} mean ± SEM (n)	V_{jct} correction	Corrected V_{rev}
		mV	*mV*	
D112V/V116D	Na^+	−1.8 ± 1.9 (4)	1.3	−0.5
	K^+	−2.3 ± 1.9 (4)	4.8	2.5
	Li^+	0.0 ± 1.0 (7)	−1.0	−1.0
	Cl^-	−1.3 ± 1.5 (4)	−3.3	−4.6
D112V/V116D/R211H	Na^+	−1.6 ± 1.8 (3)	1.3	−0.3
	K^+	−3.1 ± 1.6 (3)	4.8	1.7
	Li^+	1.5 ± 1.4 (7)	−1.0	0.5
	Cl^-	3.0 ± 2.6 (3)	−3.3	−0.3

Measurements were made at symmetrical pH 7.0, with TMA^+ or $CH_3SO_3^-$ replaced by cations or anions at concentrations of ∼100 mM. The small changes in V_{rev} were of the same order as variability and liquid junction potentials.